AGU ADVANCING EARTH AND SPACE SCIENCES

Geophysical Research Letters

RESEARCH LETTER
10.1029/2025GL120586

The Hematite Question: Hydrogen-Driven Magnetization of Hematite-Bearing Sandstones and Insights for Natural Hydrogen Exploration

B. D. L. Mendes[1], C. Cheng[1], C. Hilgers[1], and A. Kontny[1]

[1]Institute of Applied Geosciences—Structural Geology and Tectonics, Karlsruhe Institute of Technology, Karlsruhe, Germany

Key Points:

- Hydrogen reacting with hematite in natural rocks produces superparamagnetic to single-domain magnetite at low temperatures
- Hydrogen-induced hematite to magnetite reduction can increase the magnetic susceptibility of sandstones by up to three orders of magnitude
- Reduction in nature could create magnetic anomalies, which would serve as an additional indicator for natural hydrogen exploration

Supporting Information:

Supporting Information may be found in the online version of this article.

Correspondence to:

B. D. L. Mendes and C. Cheng,
bruno.mendes@kit.edu;
chaojie.cheng@kit.edu

Citation:

Mendes, B. D. L., Cheng, C., Hilgers, C., & Kontny, A. (2026). The hematite question: Hydrogen-driven magnetization of hematite-bearing sandstones and insights for natural hydrogen exploration. *Geophysical Research Letters*, *53*, e2025GL120586. https://doi.org/10.1029/2025GL120586

Received 11 NOV 2025
Accepted 16 MAR 2026

Author Contributions:

Conceptualization: B. D. L. Mendes
Data curation: B. D. L. Mendes
Formal analysis: B. D. L. Mendes
Investigation: B. D. L. Mendes
Methodology: B. D. L. Mendes, C. Cheng
Validation: B. D. L. Mendes, C. Cheng, C. Hilgers, A. Kontny
Writing – original draft: B. D. L. Mendes
Writing – review & editing: C. Cheng, C. Hilgers, A. Kontny

Abstract Natural hydrogen is a promising clean energy resource, but locating subsurface accumulations remains challenging. Aeromagnetic anomalies are increasingly utilized as a rapid and cost-effective tool for geological hydrogen prospection, particularly associated with magnetite formation during abiotic geochemical hydrogen generation through serpentinization. In this study, we investigate an alternative hydrogen-induced source of magnetic anomalies, the hematite to magnetite reduction, in hematite-bearing rocks within hydrogen reservoirs or along migration pathways. We exposed hematite-rich granites and reservoir sandstones to hydrogen at a temperature of 200°C for 10–18 days, and measured their magnetic properties before and after. Superparamagnetic to (stable) single-domain (SP-SSD) magnetite formed during the reaction, leading to magnetic susceptibility enhancement of up to three orders of magnitude in the sandstones, whereas the granite exhibited only minor increase. These results provide proof-of-concept for hydrogen-induced hematite-to-magnetite reduction at low temperatures, potentially generating localized aeromagnetic anomalies, detectable in exploration surveys.

Plain Language Summary Natural hydrogen, mainly formed by chemical reactions between rocks and underground fluids, is seen as a promising clean energy source, but locating it beneath the surface remains a major challenge. One way to search for natural hydrogen is by detecting magnetic anomalies. These may indicate the presence of magnetite, a strongly magnetic mineral that can form when hydrogen reacts with iron oxides like hematite, one of the most common iron oxides found in rocks and soils. To test this hypothesis, we exposed hematite-bearing sandstone and granite to hydrogen at a temperature of 200°C for 10–18 days, and measured their magnetic properties before and after. The reaction produced very fine magnetite particles, causing magnetic susceptibility to increase three orders of magnitude in the sandstones. These results suggest that hydrogen can significantly change the magnetic properties of natural rocks even at low temperatures, potentially creating localized magnetic anomalies that could be detected in aeromagnetic surveys, and help locate natural hydrogen flow pathways or accumulations.

1. Introduction

Natural hydrogen (NH) is increasingly viewed as a promising "silver bullet" for the clean energy transition, offering a combustion-based energy source that is both self-replenishing (e.g., Prinzhofer et al., 2018) and widely distributed (Zgonnik et al., 2020). Despite its potential, locating viable underground sources remains a major challenge.

Serpentinization is the main process generating extractable NH, producing magnetite (Fe_3O_4) as a by-product (e.g., Vitale Brovarone et al., 2020). Magnetite formation significantly enhances the magnetic properties of serpentinites (e.g., Maffione et al., 2014), potentially creating regional aeromagnetic anomalies, wherein total magnetization (M_t) strongly contrasts with the background (Figure 1a). M_t depends on induced magnetization ($M_i = \kappa * H$; H is field intensity [A/m], κ is magnetic susceptibility) and natural remanent magnetization (NRM). These anomalies can be detected using well-established geophysical techniques, and growing research is evaluating their application for NH exploration (e.g., Coleman, 2025).

Hydrogen's volatile, diffusive, and reactive nature means it migrates or reacts before accumulating in reservoirs or reaching the surface (e.g., Myagkiy et al., 2020). Identifying migration pathways and traps is therefore critical. "Fairy circles"—circular surface depressions—are often cited as seepage indicators (e.g., Ginzburg et al., 2025),

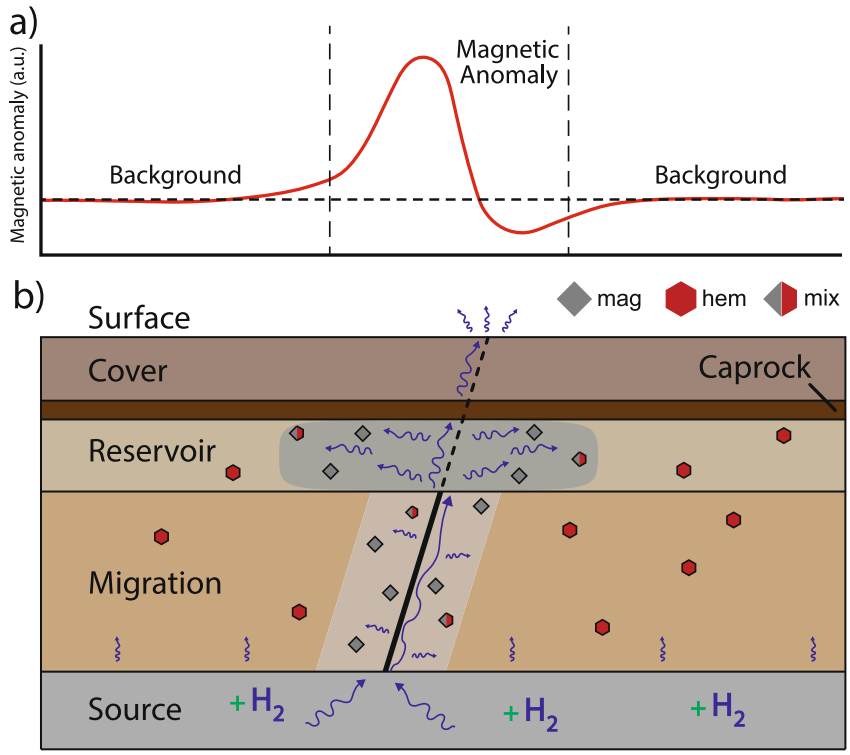

Figure 1. Conceptual sketch showing (a) a magnetic anomaly caused by hem-mag; and (b) a model of a natural hydrogen system with source, migration pathways, potential reservoirs, and surface seeps.

though their connection to subsurface reservoirs remains unclear. Migration from a source (Figure 1b) can geochemically alter host rocks (e.g., Braid et al., 2024; Cheng et al., 2025; Flesch et al., 2018), including the reduction of hematite (α-Fe_2O_3) to magnetite (hem-mag; Jozwiak et al., 2007; Thüns et al., 2019). Hematite is a canted antiferromagnetic mineral with a characteristic red color, widely distributed in geological formations. Reduction to magnetite, magnetically stronger, causes a strong increase in M_t, and can be triggered by reducing agents such as coal, hydrothermal fluids, or hydrogen (Jiang et al., 2022; Lu & Tsai, 2015).

Mendes and Kontny (2024) showed that hem-mag conversion increases κ and therefore M_i, potentially producing detectable anomalies (Figure 1). The newly formed magnetite (NFmag) exhibits (stable) single-domain (SSD) to superparamagnetic (SP) domain state behavior, overprinting the original magnetite's multidomain (MD) signal. However, these results were obtained under high temperatures (700°C) and argon atmosphere conditions (HT-Ar), leaving uncertainty about whether the reaction occurs naturally under cooler, hydrogen-rich environments (LT-H). Hematite reduction by hydrogen is well-studied in metallurgy for decarbonizing steel production 4 (e.g., Spreitzer & Schenk, 2019), but industrial processes involve continuous gas flow at 400°–1,100°C, distinct from natural environments.

To investigate the effect of hydrogen on natural hematite-bearing rocks, we exposed sandstones and martitized granites to LT-H conditions (200°C) for 10–18 days. We measured their magnetic properties before and after exposure and compared them to results from HT-Ar experiments. We then identify the main factors controlling the reaction and discuss implications for applying this phenomenon in NH exploration.

2. Materials and Methods

We selected two granite samples, one from the Soultz-sous-Forêts region, France (GS); and another from the uplifted peak-ring from the Chicxulub crater, Mexico (GC). These granites are the same material used by Mendes and Kontny (2024) to demonstrate the magnetic property changes from HT-Ar reactions.

We also selected three red-colored Triassic Buntsandstein sandstone samples, from two distinct settings: one from a Lower Buntsandstein outcrop (SO) in southern Germany (Kontny et al., 2023); and two from a natural gas

reservoir in the Northern German basin (~2.5 km depth; Cheng et al., 2025). To study how cement affects the reaction, we used two reservoir samples: one is heavily consolidated with silica-rich cement (SR-S), and the other is a more porous, "loose" material without cement (SR-L). Further details and a full sample list are in Table S1 in Supporting Information S1.

The reaction experiments were performed in hydrogen batch reactors (Cheng et al., 2025) under identical conditions (10 days at 200°C), and an initial hydrogen partial pressure of ~20 bar. Several sample sets were used to test different variables (Table S1 in Supporting Information S1):

- Set 1: rock slivers of samples SR-S, SO, GS, GC in 13 cm long test tubes ("long").
- Set 2: crushed pre-selected magnetite from granite (GS and GC), crushed sandstone (SO and SR-S) in "long" tubes. One batch ran for 18 days.
- Set 3: repetition of Set 2 (10 days) with shorter (7.4 cm) test tubes ("short").
- Set 4: "short" test tubes, SR-L sample only.

We repeated Set 2 (Set 3) because we initially used broader and longer test tubes to accommodate the rock slivers (Table S2 in Supporting Information S1). However, we later suspected that the "long" tubes may have hindered the efficient removal of the water by-product (Figure S1b in Supporting Information S1).

We expect any hem-mag reaction to occur following the equation:

$$3\ \alpha Fe_2O_3(\text{hem}) + H_2 \leftrightarrow 2\ Fe_3O_4(\text{mag}) + H_2O \quad (1)$$

Water production alters reaction kinetics, slowing or even halting it (Tang & Huang, 2022; Zhao et al., 2025). To obtain results within a reasonable timeframe, CaO powder was added to selected batch reactors in Set 1 and Set 2 (including the 18-day batch), Set 3 and Set 4. Changes in the CaO powder's mass were used to quantify the absorbed water. Further details regarding the procedures can be found in Section 1.2 of Supporting Information S1.

κ was measured using an AGICO KLY5-A susceptometer (400 A/m, 1,220 Hz). Bulk-κ measurements are mass-normalized [m^3/kg], with each sample measured three times and averaged. Temperature-dependent κ measurements (κ-T curves) were obtained only for representative sandstones, as κ-T data for the granites have been published previously (GS in Just & Kontny, 2012; GC in Mendes et al., 2023; comparison in Mendes & Kontny, 2024). In-phase and out-of-phase κ-T curves were measured under LT (−192° to 0°C) and HT (up to 700°C) conditions, using the CSL and CS4 add-on units, respectively. Out-of-phase κ in magnetite is unique to grains in the SP-SSD grain boundary for magnetite (Hrouda et al., 2022), thus any out-of-phase signal can constrain the domain state of the NFmag. For each sandstone, duplicate samples were analyzed, one before and one after the LT-H reaction. Note that κ-T curves induce the HT-Ar reaction, as described by Mendes and Kontny (2024), allowing direct comparison with the LT-H results. All data is available in SF2 (bulk-κ) and SF3 (κ-T).

3. Results

Table 1 presents mass-normalized bulk-κ results before and after the experiments and the corresponding change (m^3/kg, units are omitted in the further text for readability). Because Set 3 replicates part of Set 2, Table 1 shows only representative values; full results are in Table S3 in Supporting Information S1. After reaction, CaO powder consistently gained mass by 0.08–0.6 g (2.2%–10.6% increase), indicating uptake of by-product water. Figure 2 shows the final κ of a sample normalized to its initial value (1, dashed line), to help visualize relative variation.

Without CaO, changes in κ are minimal for the sandstones and nearly absent in the granites (Table 1). Among sandstone samples, κ increased by 3.60×10^{-10} and 9.57×10^{-10} in crushed SR-S and SO, respectively; whereas SR-S sliver showed a decrease of 2.43×10^{-9}. The CaO mass gain, along with the lack of changes in the "No CaO" batches, supports the reaction pathway in Equation 1. Consequently, we exclude the "No CaO" batches from subsequent discussion.

3.1. κ Variations in Granite and Sandstone Samples

GS samples show only minor κ changes after reaction (Figure 2a), with the largest being a 5.84×10^{-7} increase in the sliver sample. Crushed GS samples show smaller increases of 5.33×10^{-7} and 4.02×10^{-6} after 10 and

Table 1
Bulk-κ Results Before and After Reaction

Lithology	Sample	Conditions	Exposure time (days)	State	Bulk κ - mass normalized (m^3/kg)			Set and batch code
					Before	After	Change	
Granite	GS	CaO	10	Sliver	1.90E-06	2.48E-06	+5.84E-07	S1-B2
				Crushed	4.68E-05	4.73E-05	+5.33E-07	S2-B2
			18	Crushed	9.07E-05	9.47E-05	+4.02E-06	S2-B3
		No CaO	10	Sliver	8.74E-06	8.72E-06	−1.49E-08	S1-B1
				Crushed	2.34E-05	2.35E-05	+6.67E-08	S2-B1
	GC	CaO	10	Sliver	1.56E-07	1.66E-07	+9.87E-09	S1-B2
				Crushed	1.80E-05	1.68E-05	−1.17E-06	S2-B2
			18	Crushed	1.28E-05	3.08E-05	+1.80E-05	S2-B3
		No CaO	10	Sliver	3.95E-07	3.92E-07	−2.94E-09	S1-B1
				Crushed	4.04E-06	3.02E-06	−1.02E-06	S2-B1
Sandstone	SR-S	CaO	10	Sliver	2.60E-09	6.32E-09	+3.72E-09	S1-B2
				Crushed	−7.39E-10	5.28E-09	+6.02E-09	S3-B2
			18	Crushed	3.95E-09	1.27E-08	+8.75E-09	S2-B3
		No CaO	10	Sliver	4.35E-09	1.92E-09	−2.43E-09	S1-B1
				Crushed	3.44E-09	3.80E-09	+3.60E-10	S2-B1
	SR-L	CaO	10	Crushed	−4.57E-10	2.44E-07	+2.45E-07	S4
	SO	CaO	10	Sliver	4.60E-09	1.00E-08	+5.40E-09	S1-B2
				Crushed	1.67E-09	5.50E-07	+5.48E-07	S2-B2
			18	Crushed	2.25E-09	1.11E-06	+1.10E-06	S2-B3
		No CaO	10	Sliver	4.37E-09	5.55E-09	+1.18E-09	S1-B1
				Crushed	1.56E-09	2.51E-09	+9.57E-10	S2-B1

18 days, respectively (Table 1). GC samples display greater variability: after 10 days, κ increased 9.87×10^{-9} in the sliver sample but decreased by 1.17×10^{-6} in the crushed sample. After 18 days, GC exhibits the highest relative increase, although absolute κ values remain identical (1.28×10^{-5} to 3.08×10^{-5}). Section 4.1 discusses reasons for these limited variations.

Among the sandstones, SR-S is the least reactive (Figure 2b) but still shows notable κ increases: after 10 days, sliver rises by 3.72×10^{-9}, the crushed sample by 6.02×10^{-9}, and after 18 days by 8.75×10^{-9} (Table 1). Despite these relative increases, absolute κ remains low; for example, a 6.02×10^{-9} increase reflects a shift from -7.39×10^{-10} to 5.28×10^{-9}. In contrast, SR-L undergoes a strong relative κ increase of up to three orders of magnitude, from -4.57×10^{-10} to 2.44×10^{-7}, accompanied by a pronounced color change from vivid red to dark brown/black (Figure S2 in Supporting Information S1). Sample SO shows similar behavior, with consistent κ increases under all conditions. The sliver sample increases by one (5.40×10^{-9}), while crushed samples increase by up to three orders of magnitude (5.48×10^{-7} and 1.10×10^{-6} after 10 and 18 days). These crushed samples also darken noticeably (Figure S2 in Supporting Information S1). In these highly reactive sandstones, final κ reaches values comparable to magnetite-bearing granites (10^{-7} to 10^{-6} m^3/kg).

3.2. κ-T Characteristics Before and After Hydrogen Reaction

Before reaction, the initial ("heating", red line in Figures 3a–3i) in-phase κ-T curves of all sandstones are identical, showing a low, temperature-independent κ, followed by a sharp increase above 450°C and a Curie temperature (Tc) around 530°C (SR-L), 540°C (SR-S), or 560°C (SO) (Figure 3, "IP Before"). Tc was determined using the 1st derivative method (Petrovský & Kapička, 2006). Out-of-phase curves behave identically to the in-phase curves. The sharp increase above 450°C and Tc values are consistent with neoformation of magnetite (and the associated Hopkinson Peak).

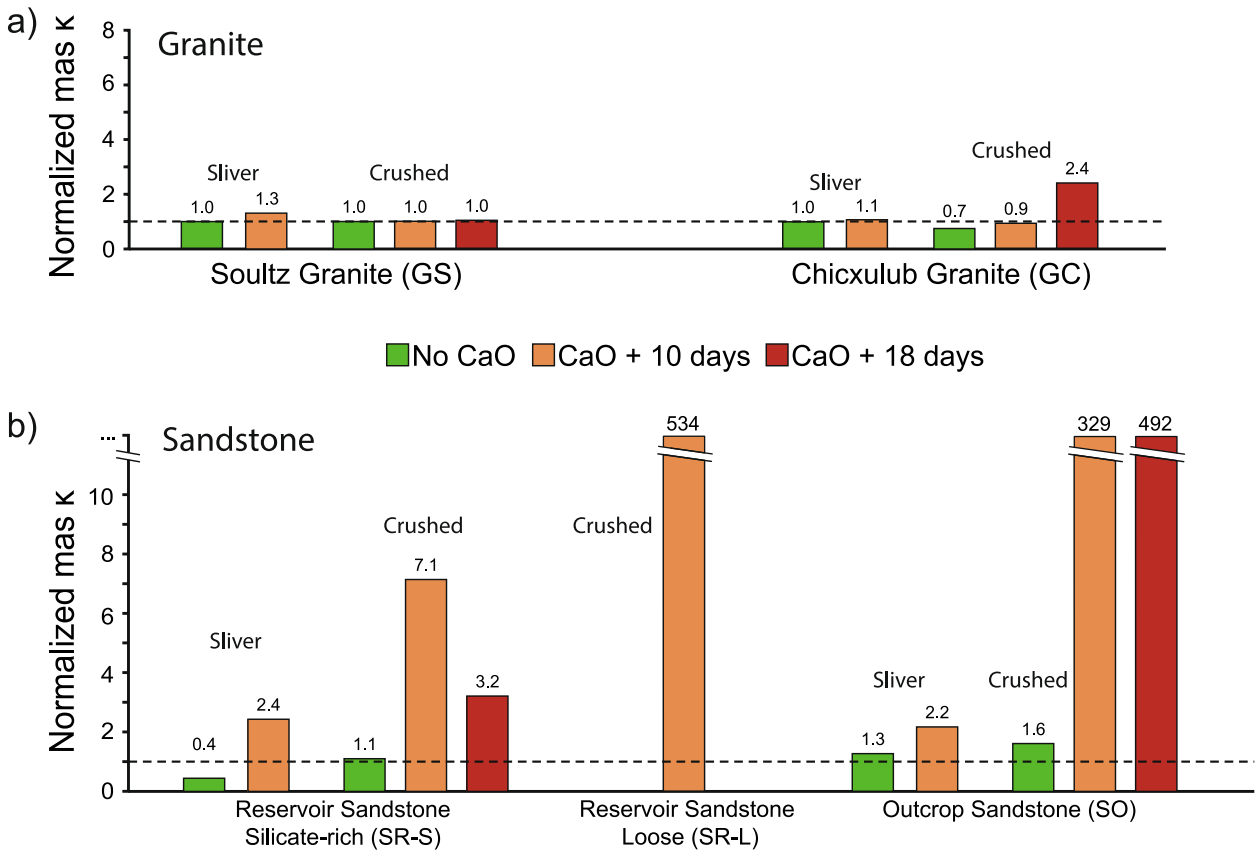

Figure 2. Comparison of κ, normalized to each sample's κ before reactions for easy visualization of κ in granites (a) and sandstones (b). Colors indicate reaction conditions.

For SR-S, the cooling curve (blue line) before reaction decreases progressively from the Hopkinson peak to a value around six times the initial κ. After reaction, both in- and out-of-phase (Figures 3b and 3c) curves exhibit only minor changes, indicating no significant alteration.

SR-L shows more pronounced changes. Before reaction (Figure 3d), the cooling curve reveals an irreversible increase in κ along with a broad hump (dashed circle) peaking around 300°C. After cooling, the final κ is around seven times higher than the initial value (Figure 3d). After reaction (Figure 3e), the initial κ is already about six times higher than before (compare red and orange lines in Figure 3k). The heating curve develops a sharp hump at 290°C (dashed circle). The cooling curve remains partially reversible above ~450°C, with a subdued, broad hump below that temperature. The final κ reaches approximately eight times the initial pre-reaction value (Figure 3k). The out-of-phase curve after reaction is fully reversible and matches the pre-reaction cooling curve (Figure 3f).

SO behaves similarly to SR-L. Before reaction (Figure 3g), the cooling curve shows a broad hump (dashed circle) with a peak temperature of around 420°C. The final κ is approximately 10 times higher than initially. After reaction, the initial κ is about six times higher than pre-reaction (Figure 3l). During heating, a sharp hump appears at 280°C (dashed circle), followed by a less pronounced hump during cooling. The final κ matches the pre-reaction cooling curve values (Figure 3l). Notoriously, a Verwey transition is observed at temperatures (Tv) of −147°C (before heating) and −157°C (after heating), confirming the presence of magnetite after the LT-H reaction. Out-of-phase curves also change: They become nearly flat and fully reversible after the reaction (Figure 3i).

No iron (Tc ~770°C) was detected in in- and out-of-phase κ after reaction (Figure 3).

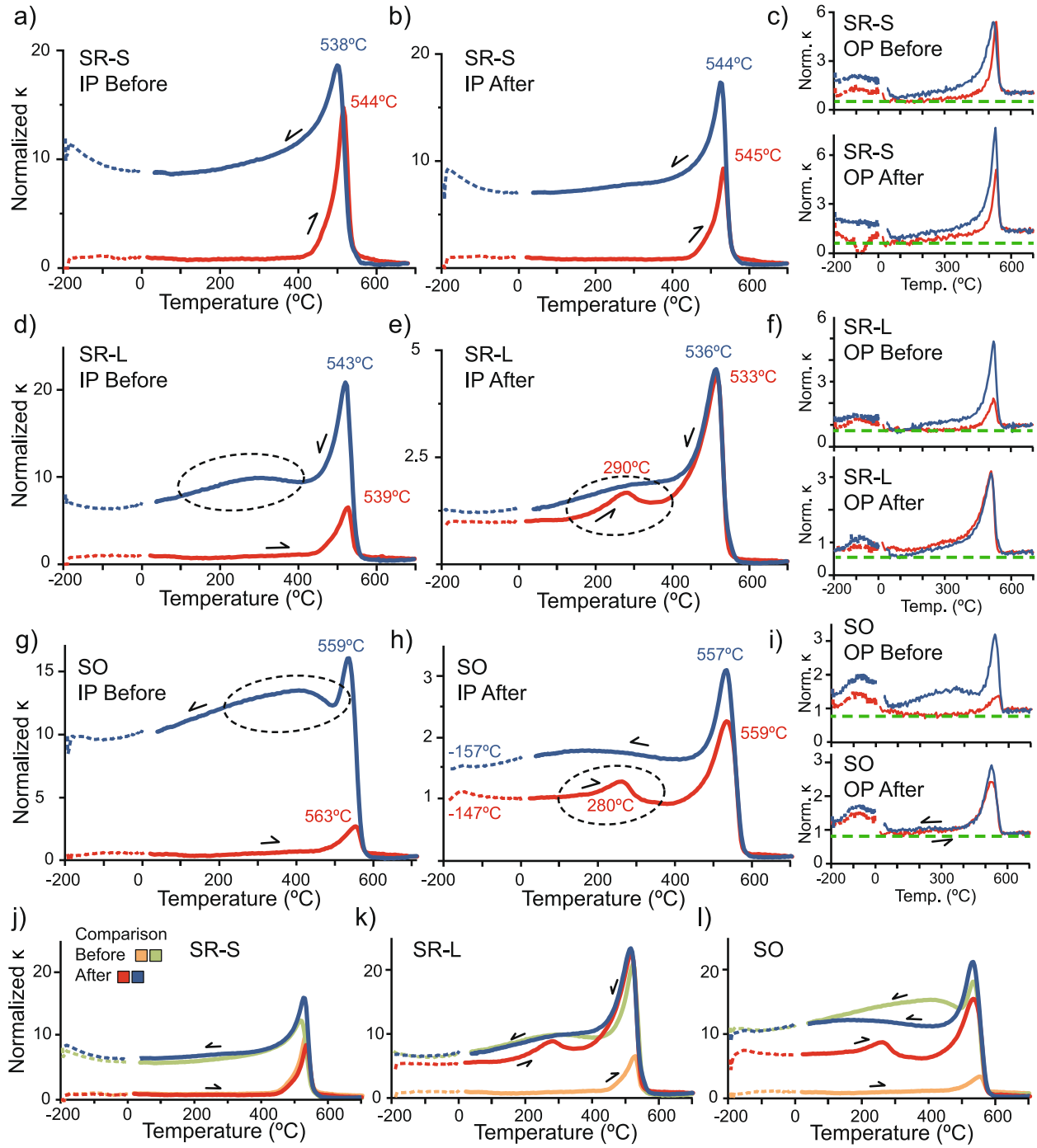

Figure 3. Normalized in-phase (IP) and out-of-phase (OP) κ-T curves for sandstones, including samples SR-S (a, b, c); SR-L (d, e, f), and SO (g, h, i). Comparison curves (j, k, l) are normalized to each sample's κ at room temperature before reaction (orange line). Humps are highlighted by dashed circles and explained in the text. In OP curves, we added an arbitrary green dashed line to highlight subtle slopes despite noise. Curie temperatures are labeled in the figure.

The non-zero out-of-phase κ in all samples results from normalization. Because absolute κ values are very low, scaling to the room-temperature value forces the curve to oscillate around 1. The only exception, sample SR-S, shows $\kappa > 600$°C exceeding its room-temperature κ, but this behavior occurs both before and after hydrogen exposure, and the sample is largely unreacted. This suggests that the anomaly is unrelated to hydrogen and is likely a correction artifact.

4. Discussion

4.1. Hydrogen-Induced Reduction in Natural Hematite-Bearing Rocks

Our results show that magnetite forms when hydrogen reduces hematite, at 200°C over 10–18 days, if water is efficiently removed (Mao et al., 2023; Tang & Huang, 2022; Zhao et al., 2025).

The initial mineralogy is a key factor controlling the reaction: granites contain abundant MD magnetite with high κ, so hem-mag reduction causes minor (relative) κ increases (Figure 2a). Previous HT-Ar experiments on the same samples report significant κ increases (1.5x initial κ), indicating the full transformation of hem to mag (Just & Kontny, 2012; Mendes et al., 2023). Overall, our granite samples show smaller κ increases (maximum 1.3x after 10 days, Figure 2a), which we attribute to incomplete hem-mag transformation and a secondary reduction reaction in which magnetite is reduced by hydrogen to wüstite (wus):

$$Fe_3O_4(mag) + H_2 \leftrightarrow 3\,FeO(wus) + H_2O \quad (2)$$

While non-stoichiometric wüstite is metastable below ~575°C (e.g., Stølen et al., 1995), recent studies document a hydrogen-induced reduction of magnetite into metallic iron in two stages: Magnetite → Wüstite → Iron, at 300°C (Zheng et al., 2023). As we have not detected iron in our κ–T curves, the 200°C conditions allow only the first decomposition stage, producing new wüstite and partial loss of the original magnetite. Because wüstite is paramagnetic at room temperature (Néel temperature approx. −73°C, Cornell & Schwertman, 2003), it lowers κ, counteracting the hem-mag induced increase, and can yield negligible or even decreased κ (Figure 2a).

Native iron can also form directly from hematite reduction (Thüns et al., 2019), but our κ–T data do not support any iron production. Native iron has a higher κ than hematite and a Tc of ~770°C. If present, κ–T curves would have show it (Figure 3).

Another major factor controlling the reaction is the effective reactive surface area. Crushed materials are consistently more reactive than rock slivers, particularly in the sandstones: slivers showed a relatively small increase in κ compared to the three orders of magnitude increases in the crushed material (Figure 2b). In the granites, slivers showed consistent κ increases, but the crushed material showed little change or even κ decreases (Figure 2a). This pattern reflects an enhanced reaction as well: in slivers, only the surface magnetite and hematite are exposed, which limits both hem-mag and magnetite-wüstite reduction. In the crushed samples, the magnetite is more exposed, so more of it reduces to wüstite. In granites with abundant magnetite compared to hematite (e.g., GC, Mendes et al., 2023), this reaction explains the overall decrease in κ. These results suggest that the effective reactive surface area strongly controls the reaction.

In the sandstone samples, the contrasting behavior between SR-S and the reactive samples SR-L and SO (Table 1, Figure 2b) is due to texture and composition, specifically the silicate cement. The cement lowers effective porosity (~11%) and permeability (131 mD), compared to SR-L (24.1% and 4,017 mD; Cheng et al., 2025). SO also has relatively low porosity and permeability (12.5%, 63 mD; Kontny et al., 2023), so these parameters alone do not explain the reactivity differences. Instead, the silicate cement in SR-S likely forms inner-sphere complexes that block or inhibit access to hematite surface-reaction sites (e.g., Stumm, 1995). As a result, SR-S is considered "unreacted": despite the minor increase in κ, its in- and out-of-phase κ-T curves show no discernible changes after LT-H exposure (Figures 3a–3c). In contrast, SR-L and SO show clear evidence of magnetite formation, including a strong κ increase, color change, sharp Tc with Hopkinson peaks, and a Tv in SO. Their suppressed Tv is consistent with SSD and (quasi-) SP particles, and the lower Tc values (530°–560°C vs. ~578°C) can also be attributed to a high fraction of particles in the SP range (Fabian et al., 2013; Wang et al., 2004). Alternatively, cation doping can also explain the observations (e.g., Harrison & Putnis, 1996; Lattard et al., 2006), in which elements like aluminum from clay minerals or the original hematite get incorporated into the NFmag. SO is likely to have lost these elements through weathering, so its NFmag will not be as substituted, explaining its higher Tc (~560°C) and visible Tv (~−152°C).

4.2. Magnetic Characterization

Before the reaction, κ-T curves show the usual irreversible increase in κ caused by hem-mag reduction in HT-Ar, as described in earlier studies (Just & Kontny, 2012; Mendes et al., 2023; Mendes & Kontny, 2024). We include the unreacted SR-S sample after LT-H treatment in this category as well.

In the reactive samples SR-L and SO, the comparison of κ-T curves before and after the experiment (Figures 3j–3l) shows that the LT-H reaction results in lower κ (red line) than the HT-Ar reaction (green line). Additionally, after LT-H treatment, the κ-T curves show a distinct hump at 280°–290°C, absent after HT-Ar treatment. One explanation for the lower κ and irreversibility is that the reaction is incomplete at LT-H, and a second heating to 700°C might help finish the transformation. This idea was proposed by Mendes et al. (2023) and Mendes and Kontny (2024) for similar observations. However, our out-of-phase κ-T curves are incompatible with this hypothesis: after HT-Ar treatment (Figures 3f and 3i; blue line "Before"), the appearance of an out-of-phase signal below 450°C indicates that this signal is carried only by the NFmag. In contrast, after LT-H treatment, the out-of-phase signal below 450°C is present before HT-Ar and remains unchanged after heating. If the reaction was incomplete, new NFmag would form after heating, causing a higher κ in the cooling curve, which is not observed. This likely also applies to the earlier studies, which lack out-of-phase data.

Another possible explanation is that heating causes maghemite to revert into hematite or cation-substituted magnetite. This has often been linked to the hump feature and irreversible changes after heating to 700°C (e.g., Deng et al., 2001; Dunlop & Özdemir, 1997; Liu et al., 2005; Vahle & Kontny, 2005). However, our data show a single Tc, indicating only one magnetic phase. Instead, we follow the explanation by Zhang and Appel (2023; based on Worm, 1998; Egli, 2009), who suggest that the hump and irreversible behavior come from a permanent change in how magnetite nanoparticles in SP-SSD clusters thermally relax when heated. After heating to 700°C, κ increases, the hump broadens and becomes less distinct, and the Hopkinson peak temperature often rises. When heating and cooling are repeated, κ stays higher, but the curves become reversible. This suggests stronger interactions between particles in the clusters, effectively making them behave like larger magnetic grains.

This interpretation is compatible with our observations. In magnetite, the out-of-phase signal derives from very small, viscous particles that are between stable and unstable magnetic states near the SP-SSD boundary (~30 nm at room temperature, Dunlop, 1973; Hrouda et al., 2022). Detecting an out-of-phase signal constrains the NFmag grains to this size range. After cooling, the sharp hump in the signal broadens, along with a permanent increase in κ (Figures 3e and 3f). Strong Hopkinson peaks in both in- and out-of-phase confirm the presence of SSD grains, and the out-of-phase signal also shows that a significant SP component forms after reactions under both HT-Ar and LT-H conditions (Figures 3c, 3f, and 3i). All in all, these effects suggest that SSD and interacting SP magnetite form under both HT-Ar and LT-H conditions alike. Differences in the κ-T curves between reactive samples reflect variations in magnetite grain size.

Based on our comprehensive results, we conclude that NFmag formed under both HT-Ar and LT-H conditions is fundamentally the same material. The higher room-temperature κ observed after HT-Ar treatment reflects thermal relaxation effects and interactions among SP-SSD clusters, rather than the formation of a new mineral phase.

4.3. Implications for Natural Hydrogen Exploration

Zhang and Appel (2023) demonstrated that SP–SSD magnetite forms from hematite in red soils during κ-T measurements under HT–Ar conditions, with First Order Reversal Curve changes consistent with those observed by Mendes et al. (2023) and Mendes and Kontny (2024). Combined with our results, these studies demonstrate that SP–SSD magnetite can form via hematite-to-magnetite transformation during laboratory κ-T experiments regardless of lithology. In natural settings, Mendes et al. (2023) reported hem–mag reduction in martitized granite from the Chicxulub crater, restricted to zones affected by high-temperature impact melts. Our experiments extend this evidence by showing that hematite-bearing sandstones can also produce NFmag with SP–SSD behavior under LT–H conditions, and that their magnetic properties resemble those formed under HT–Ar laboratory conditions (Mendes & Kontny, 2024; Zhang & Appel, 2023) and in high-temperature natural environments (Mendes et al., 2023). These results provide strong proof-of-concept that hydrogen exposure can substantially increase κ, and thus magnetization, under reservoir conditions or along migration pathways. However, further work is needed before extrapolating these findings to natural systems.

A key uncertainty is whether NFmag can carry NRM. SP magnetite cannot retain remanence (Dunlop & Özdemir, 1997), whereas SSD magnetite can acquire NRM and remains stable over geological timescales (Heider et al., 1988; Roberts et al., 2017). Establishing whether NFmag can also acquire and preserve NRM is therefore critical for assessing its contribution to magnetic anomalies.

A second major question concerns the realism of our boundary conditions. Rapid water removal by CaO accelerates hem–mag reduction in the batch experiments but may shift equilibrium away from conditions typical of fluid-rich natural systems. However, in reservoirs with continuous hydrogen inflow (e.g., Mali's "self-replenishing" system; Prinzhofer et al., 2018), hydrogen may displace existing fluids and maintain high gas saturation in the pore space. Advective hydrogen flow along migration pathways could also remove water and maintain high hydrogen chemical potential, though short exposure times of the host rock to hydrogen may conversely inhibit the reaction.

Finally, a reaction temperature of 200°C corresponds to depths of ~4–5 km (~2–3 km in geothermally active regions). Greater depths increase anomaly wavelength and reduce amplitude. A best-case estimate using the maximum sandstone κ ($\sim 10^{-6}$ kg/m^3) and a 1-km-radius body at 2 km depth yields a ~10 nT anomaly, which is detectable, but not likely diagnostic of hydrogen. Hem-mag at shallower depths could enhance detectability, but short-wavelength anomalies may be overlooked or oversmoothed in low-resolution (e.g., aircraft-based) surveys. High-resolution, targeted approaches such as drone-based surveys around features like "fairy circles" (Ginzburg et al., 2025) are therefore preferable.

5. Conclusions

Our results show that hematite-to-magnetite reduction can occur under low-temperature (200°C), hydrogen-rich conditions (LT-H), in natural hematite-bearing red sandstones and martitized granites. This reaction depends on the efficient removal of water produced during the process, requiring a low water vapor partial pressure. The resulting NFmag exhibits an effective SP-SSD domain state and is indistinguishable from NFmag formed under high-temperature argon conditions (HT-Ar) in previous studies. If similar reactions occur in natural settings, they could generate localized, high-intensity magnetic anomalies. This opens the possibility of using magnetic signals to detect NH reservoirs or migration pathways, particularly in areas with unique hydrogen-related features, such as "Fairy circles."

Conflict of Interest

The authors declare no conflicts of interest relevant to this study.

Availability Statement

The data used for this study are available at Mendes et al. (2026) [Dataset], under the name of "SF2" for bulk-susceptibility, and "SF3" for temperature-dependent susceptibility data. Both processed and raw data are available in the Mendeley Data open respository, with the https://doi.org/10.17632/rk9tysghtj.1.

Acknowledgments

C.C. and C.H. gratefully acknowledge the funding support from the German Federal Ministry of Economic Affairs and Climate Action (BMWK), SamuH2 project (Grant 03EI3051A) and the Horizon Europe HyDRA project (Grant 101192337), which enabled the establishment of the ME.Lab and facilitated the experimental investigations. C.C. also extends sincere thanks to Dr. Christian Ostertag-Henning for valuable communication and scientific discussions regarding hematite–hydrogen reactions and batch experiments. We are thankful to Mark J. Dekkers and Erwin Appel for their very constructive reviews. Open access funding enabled and organized by Project DEAL.

References

Braid, H., Taylor, K., Hough, E., Rochelle, C., Niasar, V., & Ma, L. (2024). Hydrogen-induced mineral alteration: A review in the context of underground hydrogen storage (UHS) in saline aquifers. *Earth-Science Reviews*, *259*, 104975. https://doi.org/10.1016/j.earscirev.2024.104975

Cheng, C., Busch, B., Kontny, A., & Hilgers, C. (2025). Underground hydrogen storage in sandstone reservoirs: Effects of geochemical reactivity of hydrogen on reservoir performance. *International Journal of Hydrogen Energy*, *105*, 492–504. https://doi.org/10.1016/j.ijhydene.2025.01.330

Coleman, R. (2025). Magnetic monitoring of hydrogen production during serpentinization. *Magnetic Interactions 2025*.

Cornell, R. M., & Schwertmann, U. (2003). *The iron oxides: Structure, properties, reactions, occurrences and uses*. John Wiley & Sons.

Deng, C., Zhu, R., Jackson, M. J., Verosub, K. L., & Singer, M. J. (2001). Variability of the temperature-dependent susceptibility of the Holocene Eolian deposits in the Chinese Loess plateau: A pedogenesis indicator. *Physics and Chemistry of the Earth–Part A: Solid Earth and Geodesy*, *26*(11–12), 873–878. https://doi.org/10.1016/s1464-1895(01)00135-1

Dunlop, D. J. (1973). Superparamagnetic and single-domain threshold sizes in magnetite. *Journal of Geophysical Research*, *78*(11), 1780–1793. https://doi.org/10.1029/jb078i011p01780

Dunlop, D. J., & Özdemir, Ö. (1997). *Rock magnetism: Fundamentals and frontiers (No. 3)*. Cambridge University Press.

Egli, R. (2009). Magnetic susceptibility measurements as a function of temeperature and freqeuncy I: Inversion theory. *Geophysical Journal International*, *177*(2), 395–420. https://doi.org/10.1111/j.1365-246x.2009.04081.x

Fabian, K., Shcherbakov, V. P., & McEnroe, S. A. (2013). Measuring the curie temperature. *Geochemistry, Geophysics, Geosystems*, *14*(4), 947–961. https://doi.org/10.1029/2012gc004440

Flesch, S., Pudlo, D., Albrecht, D., Jacob, A., & Enzmann, F. (2018). Hydrogen underground storage—Petrographic and petrophysical variations in reservoir sandstones from laboratory experiments under simulated reservoir conditions. *International Journal of Hydrogen Energy*, *43*(45), 20822–20835. https://doi.org/10.1016/j.ijhydene.2018.09.112

Ginzburg, N., Daynac, J., Hesni, S., Geymond, U., & Roche, V. (2025). Identification of natural hydrogen seeps: Leveraging AI for automated classification of sub-circular depressions. *Earth and Space Science*, *12*(5), e2025EA004227. https://doi.org/10.1029/2025ea004227

Harrison, R. J., & Putnis, A. (1996). Magnetic properties of the magnetite-spinel solid solution; curie temperatures, magnetic susceptibilities, and cation ordering. *American Mineralogist*, *81*(3–4), 375–384. https://doi.org/10.2138/am-1996-3-412

Heider, F., Halgedahl, S. L., & Dunlop, D. J. (1988). Temperature dependence of magnetic domains in magnetite crystals. *Geophysical Research Letters*, *15*(5), 499–502. https://doi.org/10.1029/gl015i005p00499

Hrouda, F., Chadima, M., & Ježek, J. (2022). Anisotropy of out-of-phase magnetic susceptibility and its potential for rock fabric studies: A review. *Geosciences*, *12*(6), 234. https://doi.org/10.3390/geosciences12060234

Jiang, Z., Liu, Q., Roberts, A. P., Dekkers, M. J., Barrón, V., Torrent, J., & Li, S. (2022). The magnetic and color reflectance properties of hematite: From Earth to Mars. *Reviews of Geophysics*, *60*(1), e2020RG000698. https://doi.org/10.1029/2020rg000698

Jozwiak, W. K., Kaczmarek, E., Maniecki, T. P., Ignaczak, W., & Maniukiewicz, W. (2007). Reduction behavior of iron oxides in hydrogen and carbon monoxide atmospheres. *Applied Catalysis A: General*, *326*(1), 17–27. https://doi.org/10.1016/j.apcata.2007.03.021

Just, J., & Kontny, A. (2012). Thermally induced alterations of minerals during measurements of the temperature dependence of magnetic susceptibility: A case study from the hydrothermally altered soultz-sous-forêts granite, France. *International Journal of Earth Sciences*, *101*(3), 819–839. https://doi.org/10.1007/s00531-011-0668-9

Kontny, A., Busch, B., Schenk, J., & Khasanov, I. (2023). Characterization of pore space in Permo-Triassic sandstone from SW-Germany using the anisotropy of magnetic susceptibility. *International Journal of Earth Sciences*, *112*(8), 2223–2246. https://doi.org/10.1007/s00531-023-02352-z

Lattard, D., Engelmann, R., Kontny, A., & Sauerzapf, U. (2006). Curie temperatures of synthetic titanomagnetites in the fe-ti-oFe-Ti-O system: Effects of composition, crystal chemistry, and thermomagnetic methods. *Journal of Geophysical Research*, *111*(B12). https://doi.org/10.1029/2006jb004591

Liu, Q., Deng, C., Yu, Y., Torrent, J., Jackson, M. J., Banerjee, S. K., & Zhu, R. (2005). Temperature dependence of magnetic susceptibility in an argon environment: Implications for pedogenesis of Chinese loess/palaeosols. *Geophysical Journal International*, *161*(1), 102–112. https://doi.org/10.1111/j.1365-246x.2005.02564.x

Lu, J., & Tsai, C. (2015). Reduction kinetics of hematite to magnetite under hydrothermal treatments. *RSC Advances*, *5*(22), 17236–17244. https://doi.org/10.1039/c4ra12389a

Maffione, M., Morris, A., Plümper, O., & Van Hinsbergen, D. J. (2014). Magnetic properties of variably serpentinized peridotites and their implication for the evolution of oceanic core complexes. *Geochemistry, Geophysics, Geosystems*, *15*(4), 923–944. https://doi.org/10.1002/2013gc004993

Mao, X., Hu, X., Fan, Y., & Chou, K. (2023). Effect of water vapor on the reduction kinetics of hematite powder by hydrogen-water vapor in different stages. *Journal of Mining and Metallurgy, Section B: Metallurgy*, *59*(1), 65–76. https://doi.org/10.2298/jmmb220523006m

Mendes, B. D. L., Cheng, C., Hilgers, C., & Kontny, A. (2026). The hematite question: Hydrogen-driven magnetization of hematite-bearing sandstones and insights for natural hydrogen exploration [Dataset]. *Mendeley Data*, *V1*. https://doi.org/10.17632/rk9tysghtj.1

Mendes, B. D. L., & Kontny, A. (2024). Restoration and transformation: The response of shocked and oxidized magnetite to temperature. *Journal of Geophysical Research: Solid Earth*, *129*(2), e2023JB027244. https://doi.org/10.1029/2023jb027244

Mendes, B. D. L., Kontny, A., Poelchau, M., Fischer, L. A., Gaus, K., Dudzisz, K., et al. (2023). Peak-ring magnetism: Rock and mineral magnetic properties of the Chicxulub impact crater. *Bulletin*, *136*(1–2), 307–328.

Myagkiy, A., Moretti, I., & Brunet, F. (2020). Space and time distribution of subsurface H2 concentration in so-called "fairy circles": Insight from a conceptual 2-D transport model. *BSGF-Earth Sciences Bulletin*, *191*(1), 13. https://doi.org/10.1051/bsgf/2020010

Petrovský, E., & Kapička, A. (2006). On determination of the curie point from thermomagnetic curves. *Journal of Geophysical Research*, *111*(B12). https://doi.org/10.1029/2006jb004507

Prinzhofer, A., Cissé, C. S. T., & Diallo, A. B. (2018). Discovery of a large accumulation of natural hydrogen in Bourakebougou (Mali). *International Journal of Hydrogen Energy*, *43*(42), 19315–19326. https://doi.org/10.1016/j.ijhydene.2018.08.193

Roberts, A. P., Almeida, T. P., Church, N. S., Harrison, R. J., Heslop, D., Li, Y., et al. (2017). Resolving the origin of pseudo-single domain magnetic behavior. *Journal of Geophysical Research: Solid Earth*, *122*(12), 9534–9558. https://doi.org/10.1002/2017jb014860

Spreitzer, D., & Schenk, J. (2019). Reduction of iron oxides with hydrogen—A review. *Steel Research International*, *90*(10), 1900108. https://doi.org/10.1002/srin.201900108

Stølen, S., Glöckner, R., & Grønvold, F. (1995). Nearly stoichiometric iron monoxide formed as a metastable intermediate in a two-stage disproportionation of quenched wüstite. Thermodynamic and kinetic aspects. *Thermochimica Acta*, *256*(1), 91–106. https://doi.org/10.1016/0040-6031(94)02166-l

Stumm, W. (1995). The inner-sphere surface complex: A key to understanding surface reactivity. *Aquatic Chemistry, Interfacial and Interspecies Processes*, *1*, 1–32.

Tang, Q., & Huang, K. (2022). Determining the kinetic rate constants of Fe_3O_4-to-Fe and FeO-to-Fe reduction by H_2. *Chemical Engineering Journal*, *434*, 134771. https://doi.org/10.1016/j.cej.2022.134771

Thüns, N., Krooss, B. M., Zhang, Q., & Stanjek, H. (2019). The effect of H_2 pressure on the reduction kinetics of hematite at low temperatures. *International Journal of Hydrogen Energy*, *44*(50), 27615–27625. https://doi.org/10.1016/j.ijhydene.2019.08.178

Vahle, C., & Kontny, A. (2005). The use of field dependence of AC susceptibility for the interpretation of magnetic mineralogy and magnetic fabrics in the HSDP-2 basalts, Hawaii. *Earth and Planetary Science Letters*, *238*(1–2), 110–129. https://doi.org/10.1016/j.epsl.2005.07.010

Vitale Brovarone, A., Sverjensky, D., Piccoli, F., Ressico, F., Giovannelli, D., & Daniel, I. (2020). Subduction hides high-pressure sources of energy that may feed the deep subsurface biosphere. *Nature Communications*, *11*(1), 3880. https://doi.org/10.1038/s41467-020-17342-x

Wang, J., Chen, Q., Li, X., Shi, L., Peng, Z., & Zeng, C. (2004). Disappearing of the Verwey transition in magnetite nanoparticles synthesized under a magnetic field: Implications for the origin of charge ordering. *Chemical Physics Letters*, *390*(1–3), 55–58. https://doi.org/10.1016/j.cplett.2004.04.005

Worm, H. U. (1998). On the superparamagnetic—Stable single domain transition for magnetite, and frequency dependence of susceptibility. *Geophysical Journal International*, *133*(1), 201–206. https://doi.org/10.1046/j.1365-246x.1998.1331468.x

Zgonnik, V. (2020). The occurrence and geoscience of natural hydrogen: A comprehensive review. *Earth-Science Reviews*, *203*, 103140. https://doi.org/10.1016/j.earscirev.2020.103140

Zhang, Q., & Appel, E. (2023). Reversible thermal hysteresis in heating-cooling cycles of magnetic susceptibility: A fine particle effect of magnetite. *Geophysical Research Letters*, *50*(6), e2023GL102932. https://doi.org/10.1029/2023gl102932

Zhao, L., Gao, P., Zhao, B., Kong, X., Han, Y., & Li, Y. (2025). Low-temperature hydrogen reduction of Carajás hematite: Synergistic effects of kinetics and pore evolution. *International Journal of Hydrogen Energy*, *125*, 56–66. https://doi.org/10.1016/j.ijhydene.2025.04.082

Zheng, X., Subhechchha, P., Lauren, M., Yifan, W., Rafael, A., Vilá, F. Z., et al. (2023). Correlating chemistry and mass transport in sustainable iron production. *Proceedings of the National Academy of Sciences*, *120*(43), e2305097120. https://doi.org/10.1073/pnas.2305097120